

Mechanochemical synthesis of Li-rich (Li₂Fe)SO cathode for Li ion batteries

M.A.A. Mohamed^{a,b,*}, H. A. A. Saadallah^{a,b}, I. G. Gonzalez-Martinez^a, M. Hantusch^a, M. Valldor^c, B. Büchner^a, S. Hampel^a, N. Gräßler^{a,*}

^aLeibniz Institute for Solid State and Materials Research (IFW) Dresden e.V.,
Helmholtzstraße 20, D-01069 Dresden, Germany

^bDepartment of Physics, Faculty of Science, Sohag University, 82524 Sohag, Egypt

^cDepartment of Chemistry, University of Oslo, Postbox 1033, Blindern, N - 0315 Oslo,
Norway

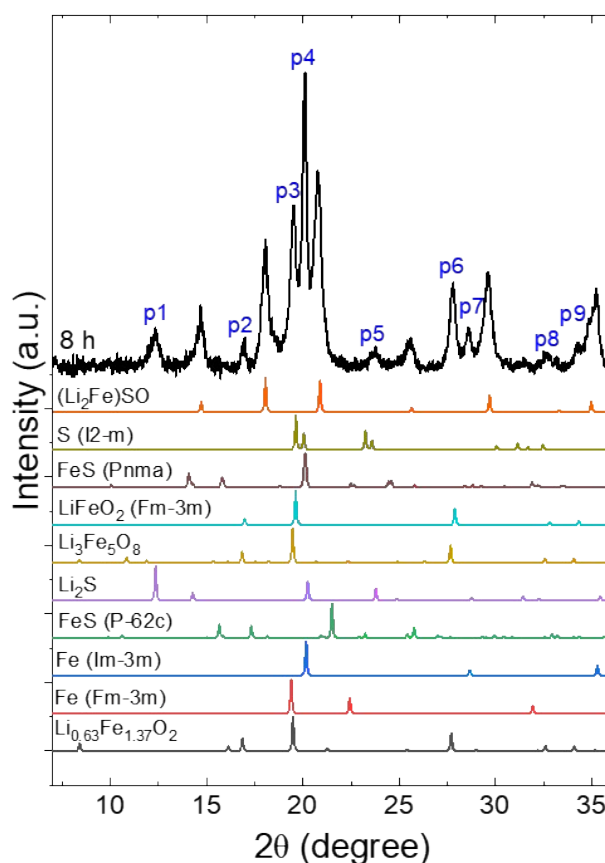


Fig S1. XRD pattern using Mo K_{α1} radiation source ($\lambda=0.70926$ Å) of the milled powder after 8 h using a 3:1 BPR. The labels from p1 to p9 refer to the peaks of the secondary phases. The XRD patterns below the sample labeled with 8 h are the references for possible phases.

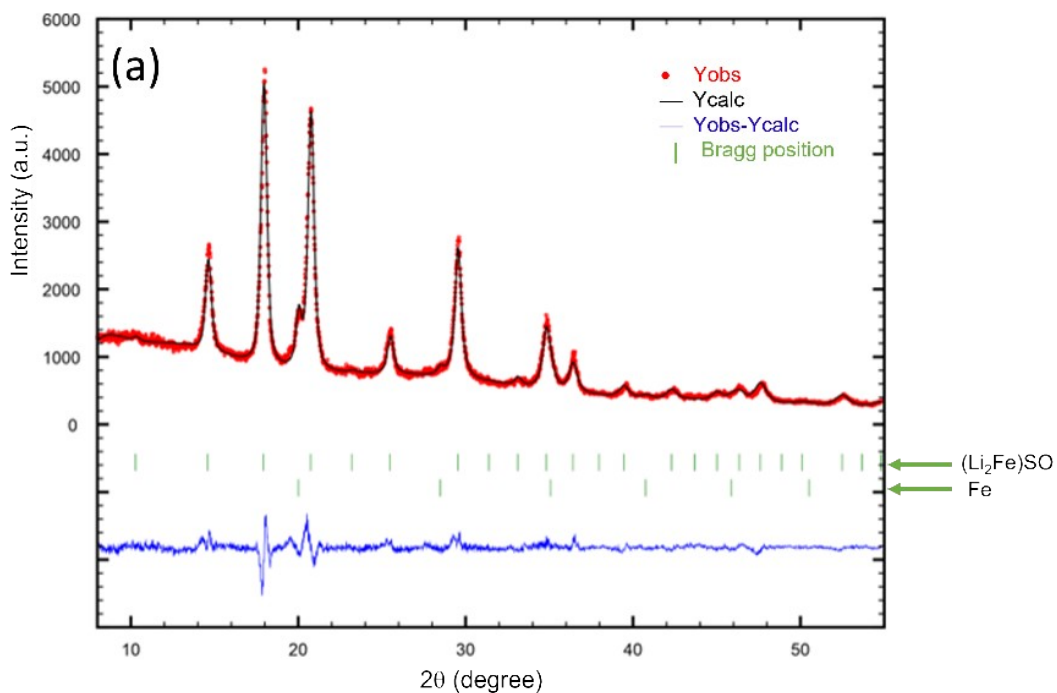


Fig. S2. Rietveld analyses for the ball-milled (Li₂Fe)SO (after 110 h milling in Fig. 2).

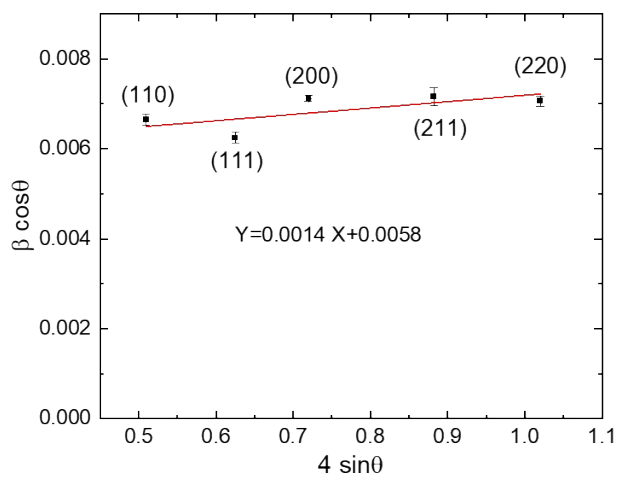


Fig. S3. W-H plot for ball-milled (Li₂Fe)SO together with the corresponding fitting equation.

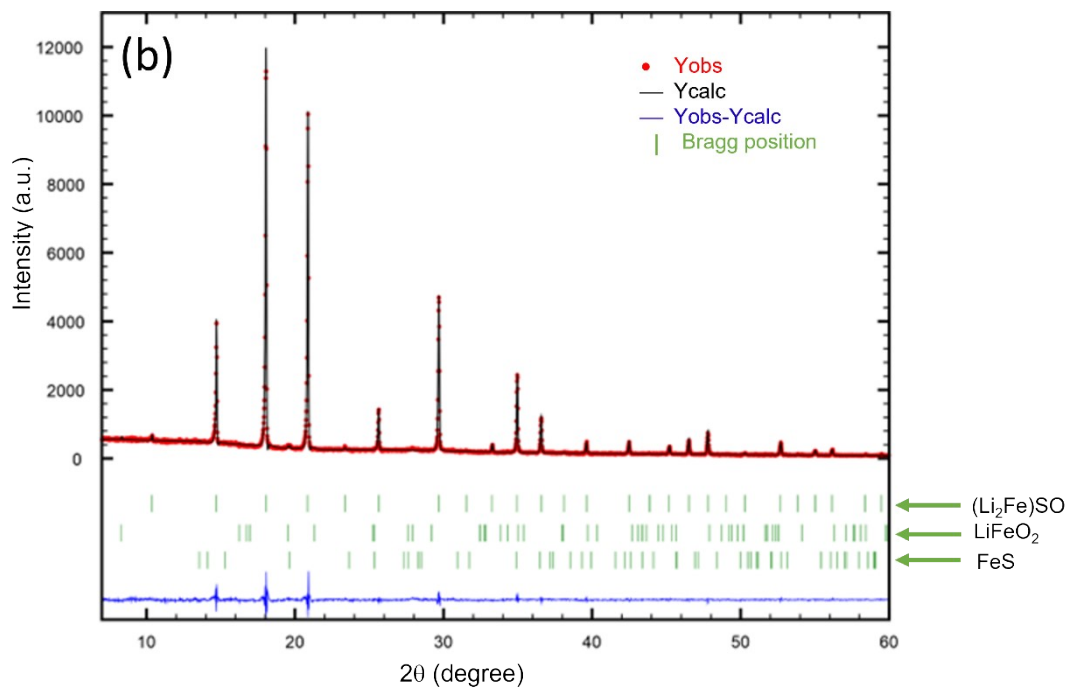


Fig. S4. Rietveld analyses for the ball-milled (Li₂Fe)SO after heat treatment at 500 °C.

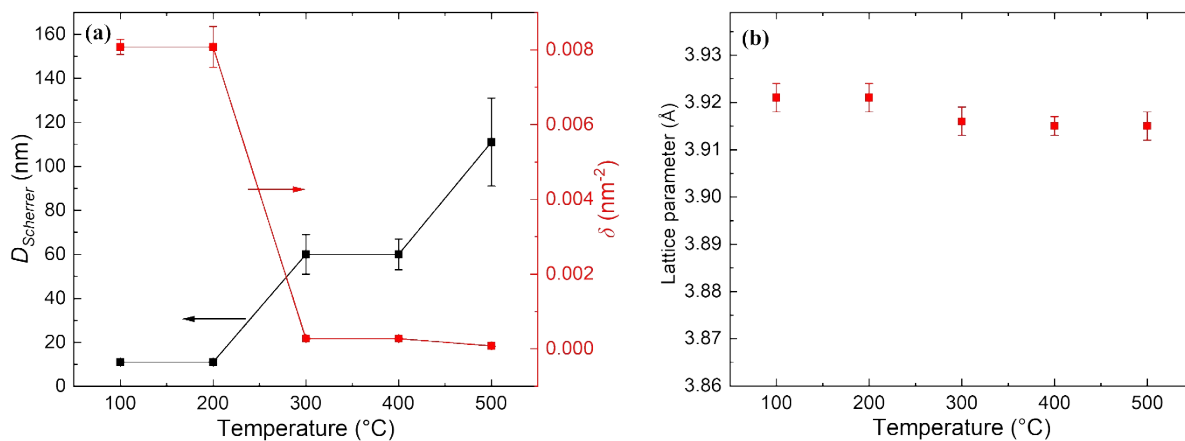


Fig. S5. Variation of Scherrer crystallite size ($D_{Scherrer}$) and dislocations density (δ) (a) and lattice parameter (b), as a function of the subsequent heat treatment temperature of the ball-milled (Li₂Fe)SO.

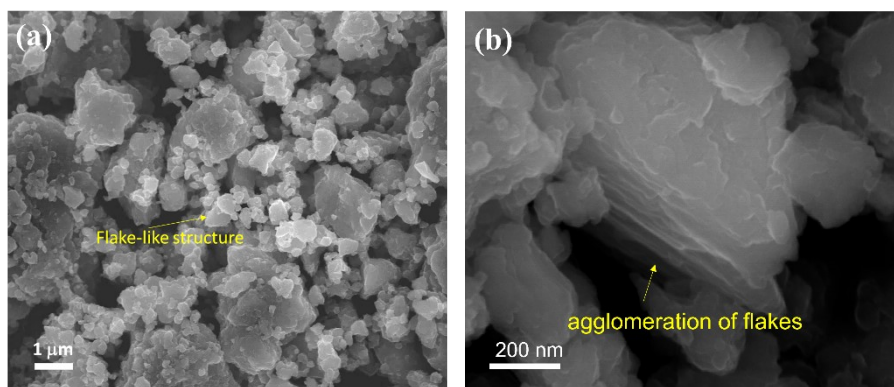


Fig. S6. Flake-like structures of ball-milled $(\text{Li}_2\text{Fe})\text{SO}$.

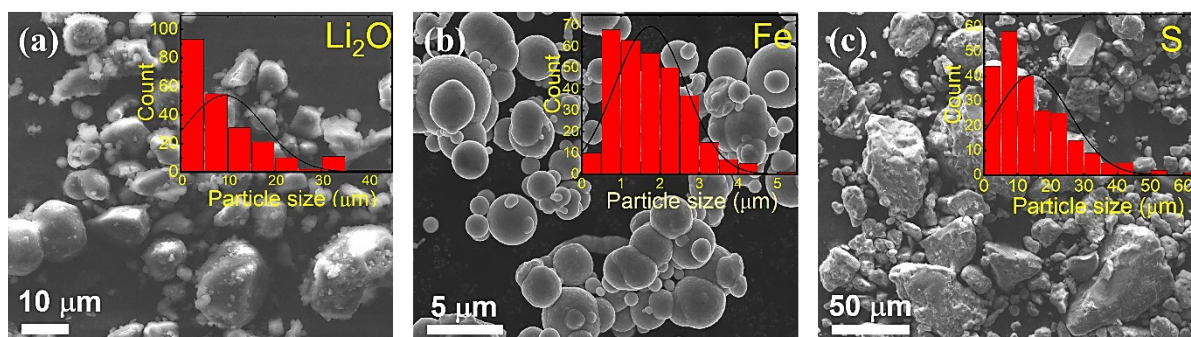


Fig. S7. SEM images of the raw materials (Li_2O , Fe, and S) used in the synthesis of $(\text{Li}_2\text{Fe})\text{SO}$. The insets represent the corresponding particle size distributions.

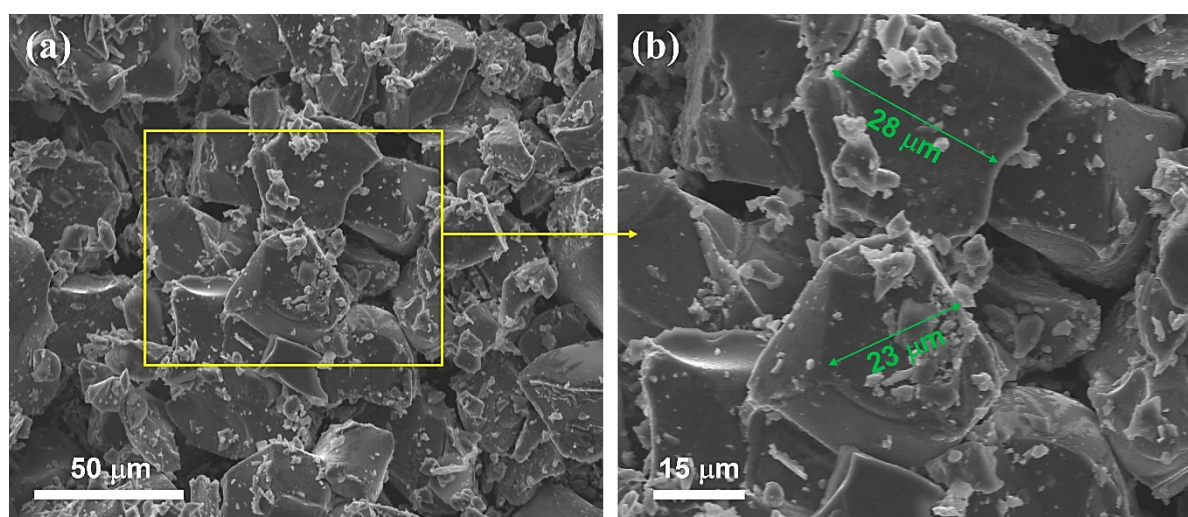


Fig. S8. SEM images for $(\text{Li}_2\text{Fe})\text{SO}$ prepared by solid state reaction method. The synthesis was reproduced from ref.1.¹

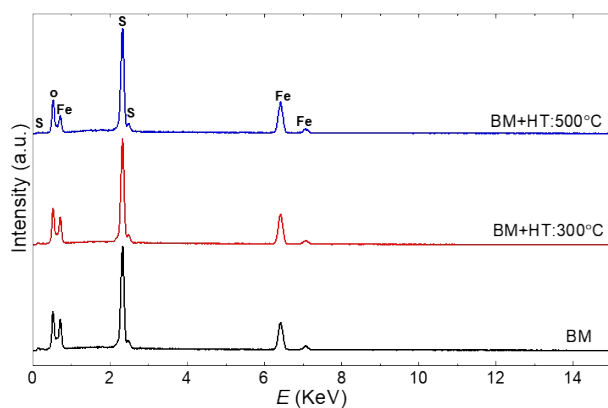


Fig. S9. EDS for ball-milled $(\text{Li}_2\text{Fe})\text{SO}$ (black) and ball-milled $(\text{Li}_2\text{Fe})\text{SO}$ followed by post-heat treatment at $300\text{ }^\circ\text{C}$ (red) and $500\text{ }^\circ\text{C}$ (blue).

composition	conditions	Atomic %		
		Fe	S	O
$(\text{Li}_2\text{Fe})\text{SO}$	ball milling	32.2 ± 1.61	32.69 ± 1.63	35.11 ± 1.76
	ball milling+heat treatment ($300\text{ }^\circ\text{C}$; 3 h)	34.32 ± 1.72	33.05 ± 1.65	32.63 ± 1.63
	ball milling+heat treatment ($500\text{ }^\circ\text{C}$; 3 h)	33.68 ± 1.68	33.56 ± 1.68	32.75 ± 1.64

composition	conditions	Mass%			Molar ratios			
		Li	Fe	S	Li	Fe	S	O
$(\text{Li}_2\text{Fe})\text{SO}$	ball milling	11.4(4)	47.3(2)	26.6(6)	1.94(6)	0.99(1)	0.98(2)	1.09
	ball milling + heat treatment ($500\text{ }^\circ\text{C}$ -3h)	11.5(1)	47(2)	25.9(5)	1.93(2)	0.98(5)	0.94(2)	1.15

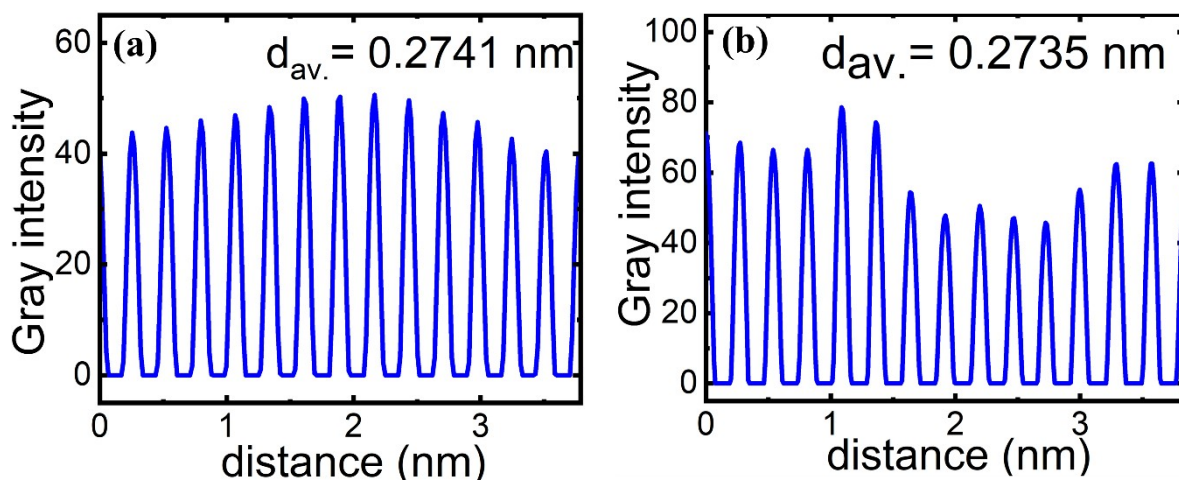


Fig. S10. Plot profile based on inverse Fourier transformation (FT) analysis for ball-milled $(\text{Li}_2\text{Fe})\text{SO}$ and (a) ball-milled $(\text{Li}_2\text{Fe})\text{SO}$ followed by post-heat treatment at 500°C (b).

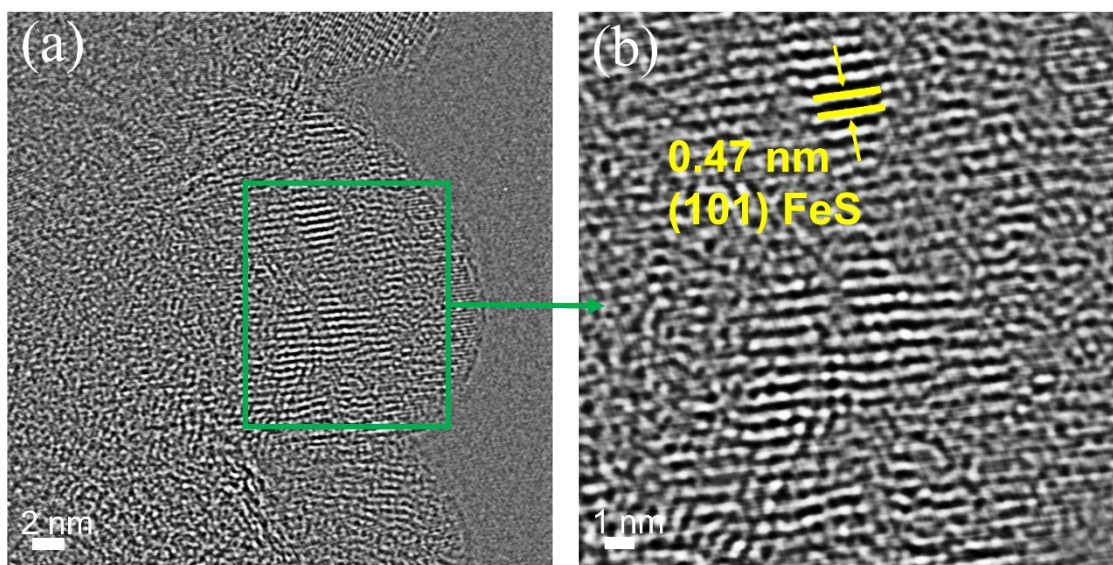


Fig. S11. Appearance of minor FeS impurity phase in the TEM images of heat-treated (at 500°C) ball-milled $(\text{Li}_2\text{Fe})\text{SO}$.

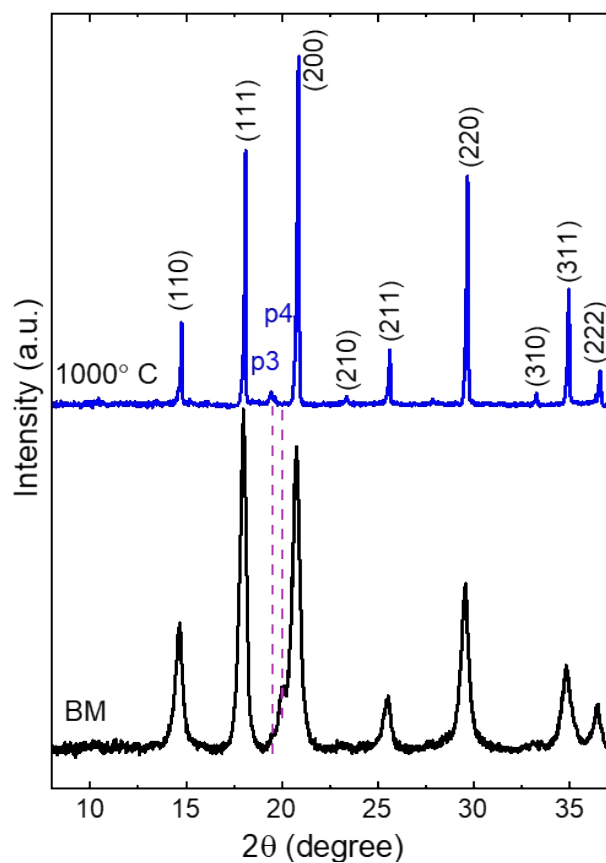


Fig. S12. XRD (using Mo $K_{\alpha 1}$ radiation source ($\lambda=0.70926 \text{ \AA}$) for ball-milled $(\text{Li}_2\text{Fe})\text{SO}$ (black) and ball-milled $(\text{Li}_2\text{Fe})\text{SO}$ followed by post-heat treatment at 1000°C (blue).

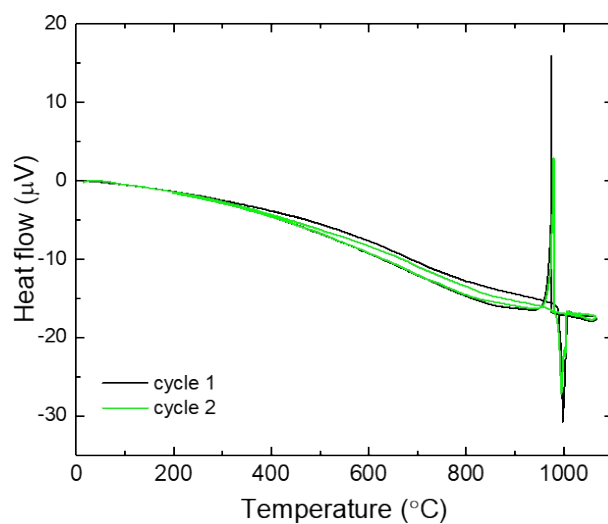


Fig. S13. DTA for ball-milled $(\text{Li}_2\text{Fe})\text{SO}$ followed by post-heat treatment at 500°C .

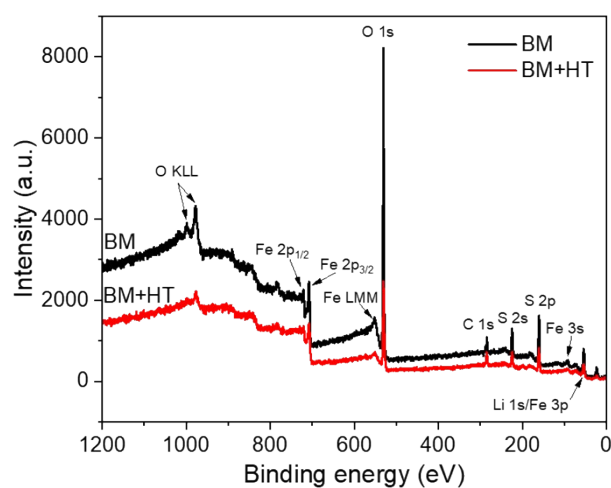


Fig. S14: Full XPS spectra for $(\text{Li}_2\text{Fe})\text{SO}$ synthesized by ball milling (BM) and ball milling followed by post-heat treatment at 500°C (BM+HT).

Table S3. Overview of selected properties of the antiperovskite (Li₂Fe)SO material and current commercialized cathode materials.^{2–9}

Composition (Research time)	Structure	Theoretical capacity ^a (mAh g ⁻¹)	Practical capacity (mAh g ⁻¹)	Voltage plateau (V)	Li ⁺ diffusion	Cost	Toxicity	Safety	Synthesis
LiCoO ₂ (LCO) (1980)	Layered	274	140-155	3.8	2D	High	High	Low	Easy
LiMn ₂ O ₄ (LMO) (1983)	Spinel	148	100-120	4.1	3D	Low	Low	Medium	Easy
LiFePO ₄ (LFP) (1997)	Olivine	170	170	3.4	1D	Low	Low	High	Medium
LiNi _{1/3} Mn _{1/3} Co _{1/3} O ₂ (NMC333) LiNi _{0.8} Co _{0.15} Al _{0.05} O ₂ (NCA) (1999)	Layered	~280	155-200	3.7	2D	Medium	Medium	Medium	Medium
(Li ₂ Fe)SO* (2017)	Antiperovskite	455	~280	2.5	3D	Low	Medium ^b	High	Easy

^a The theoretical capacity calculated corresponds to a complete extraction/insertion of Li-ion of the structure, with two Li-ions for antiperovskite (Li₂Fe)SO and one Li-ion for other cathode materials.

^b When considering only the heavy metal content, (Li₂Fe)SO is classified as "low" similar to LMO and LFP. When taking the sulfur content into account, we have ordered it as "medium". The specific conversion of sulfur into certain species after the degradation or battery recycling process is unclear as there are no studies available.

* Current commercialized cathode materials such as LiCoO₂, LiNi_{1/3}Mn_{1/3}Co_{1/3}O₂, LiNi_{0.8}Co_{0.15}Al_{0.05}O₂, LiMn₂O₄ and LiFePO₄ have some drawbacks despite their intensive optimization (see Table S3).^{3–9} These cathodes depend mainly on the intercalation chemistry of Li⁺ during electrochemical cycling. The intercalation chemistry is theoretically limited by the number of Li⁺ moles per formula unit and the available redox states of the transition metal, which is usually restricted by one electron transfer.¹⁰ The capacity of the intercalation cathodes is currently approaching its theoretical edge, which limits the energy density and represents a major hurdle. One approach to overcome such obstacle and increase the theoretical capacity is to use Li-rich cathodes with the multi-electron storage capability.¹⁰ Li-rich oxides are attractive option to get access to multi-electron storage by involving cationic (transition metal) and anionic (oxygen) redox processes.¹¹ Nevertheless, triggering O 2p oxidation requires a high voltage which is outside the electrochemical stability of organic carbonate electrolyte.¹² Although multi-electron storage was indicated by the measured specific capacity in Li-rich oxides, other irreversible degradation reactions such as O₂ gas release and electrolyte decomposition was reported to contribute to the delivered capacity.^{13,14} Instead, sulphides (S 3p) oxidize at lower voltage compared to oxides (O 2p) because of their higher energy frontier orbitals and therefore present a chance for multi-electron storage with avoiding the irreversible side reactions.^{10,12} One Li-rich system which depends on sulfide S 3p redox (anionic) along with the transition metal Fe 4p redox (cationic) is the antiperovskite (Li₂Fe)SO.² The table shows a strong interest in new cathode materials that combine high specific capacity, environmental friendliness, low cost, and high cut-off potential due to the specific disadvantages of current materials. We recognize that it is difficult to make a quantitative comparison between the novel antiperovskite material, which is still in the early stages of research. Therefore, specific parameters have been evaluated and the properties of the (Li₂Fe)SO material have been considered to the best of our knowledge. Note that the electrochemical performance of (Li₂Fe)SO cathode material synthesized by solid state reaction was used in Table S3.²

References

- 1 K. T. Lai, I. Antonyshyn, Y. Prots and M. Valldor, *J. Am. Chem. Soc.*, 2017, **139**, 9645–9649.
- 2 D. Mikhailova, L. Giebeler, S. Maletti, S. Oswald, A. Sarapulova, S. Indris, Z. Hu, J. Bednarcik and M. Valldor, *ACS Appl. Energy Mater.*, 2018, **1**, 6593–6599.
- 3 X. Shen, X. Q. Zhang, F. Ding, J. Q. Huang, R. Xu, X. Chen, C. Yan, F. Y. Su, C. M. Chen, X. Liu and Q. Zhang, *Energy Mater. Adv.*, 2021, **2021**, 1-15
- 4 P. Guan, L. Zhou, Z. Yu, Y. Sun, Y. Liu, F. Wu, Y. Jiang and D. Chu, *J. Energy Chem.*, 2020, **43**, 220–235.
- 5 N. Nitta, F. Wu, J. T. Lee and G. Yushin, *Mater. Today*, 2015, **18**, 252–264.
- 6 H. Li and H. Zhou, *Chem. Commun.*, 2012, **48**, 1201–1217.
- 7 A. Butt, G. Ali, K. Tul Kubra, R. Sharif, A. Salman, M. Bashir and S. Jamil, *Energy Technol.*, 2022, **10**, 2100775.
- 8 F. Wu, J. Maier and Y. Yu, *Chem. Soc. Rev.*, 2020, **49**, 1569–1614.
- 9 Y. Lu, Q. Zhang and J. Chen, *Sci. China Chem.*, 2019, **62**, 533–548.

- 10 C. J. Hansen, J. J. Zak, A. J. Martinolich, J. S. Ko, N. H. Bashian, F. Kaboudvand, A. Van Der Ven, B. C. Melot, J. Nelson Weker and K. A. See, *J. Am. Chem. Soc.*, 2020, **142**, 6737–6749.
- 11 W. Zuo, M. Luo, X. Liu, J. Wu, H. Liu, J. Li, M. Winter, R. Fu, W. Yang and Y. Yang, *Energy Environ. Sci.*, 2020, **13**, 4450–4497.
- 12 S. Saha, G. Assat, M. T. Sougrati, D. Foix, H. Li, J. Vergnet, S. Turi, Y. Ha, W. Yang, J. Cabana, G. Rousse, A. M. Abakumov and J. M. Tarascon, *Nat. Energy*, 2019, **4**, 977–987.
- 13 S. E. Renfrew and B. D. McCloskey, *ACS Appl. Energy Mater.*, 2019, **2**, 3762–3772.
- 14 J. Rana, J. K. Papp, Z. Lebens-Higgins, M. Zuba, L. A. Kaufman, A. Goel, R. Schmuck, M. Winter, M. S. Whittingham, W. Yang, B. D. McCloskey and L. F. J. Piper, *ACS Energy Lett.*, 2020, **5**, 634–641.